Molecular Crystals and Liquid Crystals

Publication details, including instructions for authors and subscription information:
http://www.tandfonline.com/loi/gmcl20

An Adiabatic Scanning Calorimetry Study of the Nematic-Smectic A and Nematic-Isotropic Phase Transitions in 4-butyloxyphenyl-4′-decyloxybenzoate

K. Denolf [a] , B. Van Roie [a] , C. Glorieux [a] , J. Thoen [a] , S. Yildiz [b] & H. Özbek [b]

[a] Laboratorium voor Akoestiek en Thermische Fysica, Departement Natuurkunde en Sterrenkunde, Katholieke Universiteit Leuven, Leuven, Belgium

[b] Physics Department, Istanbul Technical University, Maslak, Istanbul, Turkey

Version of record first published: 22 Sep 2010

To cite this article: K. Denolf, B. Van Roie, C. Glorieux, J. Thoen, S. Yildiz & H. Özbek (2007): An Adiabatic Scanning Calorimetry Study of the Nematic-Smectic A and Nematic-Isotropic Phase Transitions in 4-butyloxyphenyl-4′-decyloxybenzoate, Molecular Crystals and Liquid Crystals, 477:1, 3/[497]-16/[510]

To link to this article: http://dx.doi.org/10.1080/15421400701732316

Mol. Cryst. Liq. Cryst., Vol. 477, pp. 3/[497]–16/[510], 2007

ISSN: 1542-1406 print/1563-5287 online
DOI: 10.1080/15421400701732316

Taylor & Francis
Taylor & Francis Group

An Adiabatic Scanning Calorimetry Study of the Nematic-Smectic A and Nematic-Isotropic Phase Transitions in 4-butyloxyphenyl-4′-decyloxybenzoate

K. Denolf
B. Van Roie
C. Glorieux
J. Thoen
Laboratorium voor Akoestiek en Thermische Fysica, Departement Natuurkunde en Sterrenkunde, Katholieke Universiteit Leuven, Leuven, Belgium

S. Yildiz
H. Özbek
Physics Department, Istanbul Technical University, Maslak, Istanbul, Turkey

In this adiabatic scanning calorimetry (ASC) study we investigated the liquid crystal 4-butyloxyphenyl-4′-decyloxybenzoate ($\overline{1}0O\overline{4}$) with the emphasis on the nematic-to-smectic A (N-SmA) and the nematic-to-isotropic (N-I) phase transitions. Because of the high resolution ASC technique we were able to accurately determine the latent heat of the first order N-I transition. The N-SmA transition was found to be a continuous one within the experimental resolution and the value of the effective specific heat capacity critical exponent, α, was found to be 0.23 ± 0.01, thus between the 3D XY and tricritical value.

Keywords: 4-butyloxyphenyl-4'-decyloxybenzoate, $\overline{1}0O\overline{4}$, Adiabatic Scanning Calorimetry, Nematic, Smectic A

1. INTRODUCTION

Phase transitions are encountered in all levels of physics, from everyday-life phenomena to the latest state-of-the-art theoretical calculations.

Address correspondence to Jan Thoen, Laboratorium voor Akoestiek en Thermische Fysica, Departement Natuurkunde en Sterrenkunde, Katholieke Universiteit Leuven, Celestijnenlaan 200D, Leuven B-3001, Belgium. E-mail: Jan.Thoen@fys.kuleuven.be

Since liquid crystals exhibit a wide variety of mesophases and phase transitions between the liquid and the solid phase, the study of phase transitions in liquid crystals has been an interesting topic of research during the last three decades.

In the past several studies concerning the liquid crystal 4-butyloxyphenyl-4′-decyloxybenzoate ($\overline{1}0O\overline{4}$) were performed. This liquid crystal contains three mesophases between the liquid, isotropic phase and the solid, crystalline phase: the nematic, smectic A and the smectic C phase. The SmA-SmC transition in this liquid crystal was studied using high resolution X-ray scattering measurements [1]. Also binary mixtures of 4-butyloxyphenyl-4′-decyloxybenzoate and methylchloropentanoyloxyheptyloxybiphenyl (C7/B7) were investigated extensively with the focus on the smectic A-to-smectic C* phase transition [2–4]. However, no studies were reported on the nematic-to-smectic A (N-SmA) and the nematic-to-isotropic (N-I) phase transitions in this liquid crystal.

Generally, a phase transition can be classified as a first order or a continuous one, based on the behavior of the suited thermodynamic potential (the Gibbs free energy) near the transition. First order phase transitions are characterized by a discontinuity in the first derivative of the Gibbs free energy, G, with respect to the pressure, p, or the temperature, T, while continuous (second order) phase transitions show an anomaly or a finite cusp in the second derivative of G with respect to its parameters p or T [5,6]. During the adiabatic scanning calorimetry (ASC) measurements performed in this study pressure is kept constant and temperature is slowly scanned and accurately measured as a function of time. From these $T(t)$ data, the specific heat capacity, $c_p(T)$, and the enthalpy, $H(T)$, as a function of temperature can be determined. The enthalpy will exhibit a discrete jump, also called the latent heat ΔH_L, at a first order phase transition. A continuous transition, as the name implies, will show a continuous course of the enthalpy as a function of temperature.

ASC is the only calorimetric technique which is able to determine the specific heat capacity and the enthalpy directly. Therefore it is not surprising that this high resolution technique has played a major innovative role in the investigation of phase transitions in liquid crystals since the early eighties [7–9]. During the last five to ten years a new implementation of the AC calorimetric technique was developed: the photopyroelectrical (PPE) AC calorimetric technique. This technique can perform high resolution measurements of the specific heat capacity on a small sample in a very simple way [10,11].

In this article ASC measurements of the nematic-to-isotropic (N-I) and nematic-to-smectic A (N-SmA) phase transitions in $\overline{1}0O\overline{4}$ will be discussed. Photopyroelectrical AC calorimetric measurements, also

carried out in our laboratory, of the N-SmA transition in $\overline{10}O\bar{4}$ will be compared with the ASC measurements of this phase transition.

2. EXPERIMENTAL TECHNIQUES

2.1. Adiabatic Scanning Calorimetry

Adiabatic Scanning Calorimetry (ASC) is a high resolution technique which is able to measure continuously the heat capacity and the enthalpy of a sample of interest as a function of temperature. The

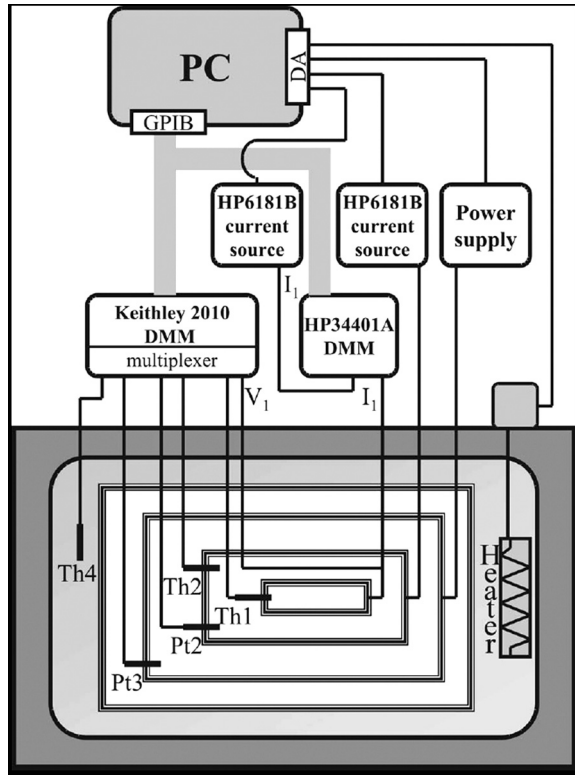

FIGURE 1 Schematic overview of the adiabatic scanning calorimeter (ASC) used in this study. The ASC consists of 3 different stages. The first stage is the sample holder including a heating coil and a thermistor to control its temperature. A shield which is also surrounded by a heating coil forms the second stage. This second stage contains a thermistor and a platinum resistance thermometer to measure its temperature. Stage 3 is a shield without heating coil which is temperature controlled by a thermistor and thermostat water bath.

adiabatic scanning calorimeter used in this study consists of a cylindrical sample holder which is surrounded by two shields as shown in Figure 1. The sample holder is made of tantalum, a thermally good conductive and a chemically inert material and it contains a thermistor thermometer and a heating coil to control its temperature. Each shield surrounding the holder is made of thermally good conductive material in order to eliminate temperature gradients. An electrical power can be applied to the first shield by means of a heating coil and its temperature can be determined by a thermistor or a platinum resistance thermometer. The temperature of the second shield is controlled by a water thermostat bath. In order to avoid heat leaks from the different stages to the environment the space between the different stages is evacuated and the connections between two successive stages are kept as small as possible.

There are two possible scanning modes: a heating run or a cooling run. The scanning rates in both modes are very small in order to maintain the thermodynamical equilibrium in the sample: typically 15 mK/min to obtain a broader view of a certain phase transition and 2 down to 0.5 mK/min to obtain a detailed zoom of a transition. If necessary the sample can also be stirred during the scans to optimize the sample homogeneity.

Upon heating a known electrical power is continuously applied to the sample holder. In order to create an adiabatic environment the first shield is kept at the same temperature as the sample holder and the temperature difference between the first and second shield is kept constant. The heat capacity of the sample of interest, C_s, can be obtained from the total heat capacity C:

$$C = C_h + C_s = \frac{P}{\dot{T}} = \frac{P^{el} + P^{leak}}{\dot{T}} \tag{1}$$

with C_h and C_s the heat capacity of respectively the sample holder and the sample, P^{el} the known applied electrical power, P^{leak} the power that flows away because of possible heat leaks in the system and $\dot{T} = dT/dt$. The heat capacity of the sample holder, C_h, can be determined by a calibration measurement. P^{leak} is virtually zero during a heating run, while during cooling no electrical power, P^{el}, but a constant negative leak power, P^{leak}, is continuously applied to the sample by keeping the first shield at a slightly lower temperature than the sample holder. By numerically differentiating the measured $T(t)$ data, $\dot{T}$ can be calculated. The specific heat capacity of the investigated sample can be obtained by dividing the heat capacity of the sample C_s by the sample mass.

Adiabatic scanning calorimetry is the only calorimetric technique that can measure the enthalpy directly. The enthalpy of the investigated sample can be obtained by inverting the measured $T(t)$ data since:

$$H(T) - H(T_s) = P(t(T) - t(T_s)), \tag{2}$$

with T_s the starting temperature of the run. Thus the latent heat of a phase transition, if present, can be determined and one will be able to classify the phase transition as a continuous or a first order one. More information about this technique can be found in literature [7,9].

2.2. Photopyroelectric AC Calorimetry

In AC calorimetry a sample of interest is heated periodically and the temperature as a function of time is measured by a thermometer. The principle of photopyroelectrical (PPE) AC calorimetry is the same, except that this technique uses a photopyroelectrical sensor instead of a thermometer. Such a photopyroelectrical transducer has the characteristic that a change in its temperature distribution, $\theta(x, t_0)$, causes a change in its polarization $\vec{P}$. This creates a net charge over the transducer given by

$$q(t) = \frac{pA}{L_P} \int_0^{L_p} [\theta_p(x,t) - \theta(x,t_0)]dx. \tag{3}$$

In this expression p is the pyroelectrical coefficient of the material, A is the area, L_p is the thickness of the sensor and $\theta(x, t_0)$ is a reference temperature distribution. With $\theta_p(t)$ the average temperature of the transducer, Eq. (3) can be written as:

$$q(t) = \frac{pA}{L_p}\theta_p(t). \tag{4}$$

Equation (4) implies that a change in sensor temperature generates an electrical current

$$i_p(t) = pA\frac{d\theta_p(t)}{dt}, \tag{5}$$

and a periodic signal generates a voltage:

$$V(\omega) = H(\omega)pA\bar{\theta}(\omega)e^{i\omega t} \tag{6}$$

with $H(\omega)$ an electrical transfer function.

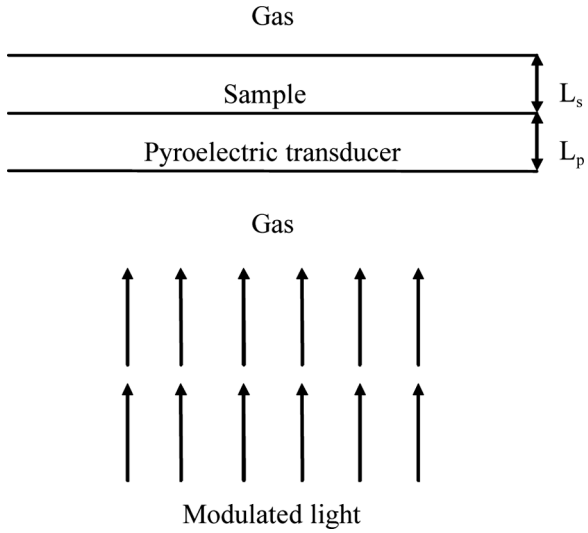

FIGURE 2 One dimensional inverse photopyroelectric geometry (front detection configuration).

Figure 2 shows schematically the so-called one dimensional inverse PPE geometry (front detection). A small drop of sample is smeared out on top of the photopyroelectrical transducer, which is illuminated from below by a Helium-Neon laser. The PZT transducer used in this setup has a diameter of 2 cm and a thickness of 200 μm. On both sides of the transducer contacts were soldered to establish the electrical signal connection. Since the thickness of the sample and the sensor is much less than their diameter, the system can be described by a one dimensional model. The variation of the (complex) temperatures can be found by solving the thermal diffusion equations and the continuity conditions for the different layers. This allows the calculation of the spatial average of the temperature in the pyroelectric transducer [10].

At low modulation frequencies, both sample and sensor become thermally very thin (sample and transducer thicknesses are much smaller than the thermal diffusion lengths L_s and L_p). At these low frequencies, the thermal waves inside sample and sensor are virtually not damped. One obtains for the average temperature in the pyroelectrical transducer [10]:

$$\theta(\omega) = \frac{I_0}{4\pi i f} \frac{-1}{\rho_s C_s L_s + \rho_p C_p L_p}. \tag{7}$$

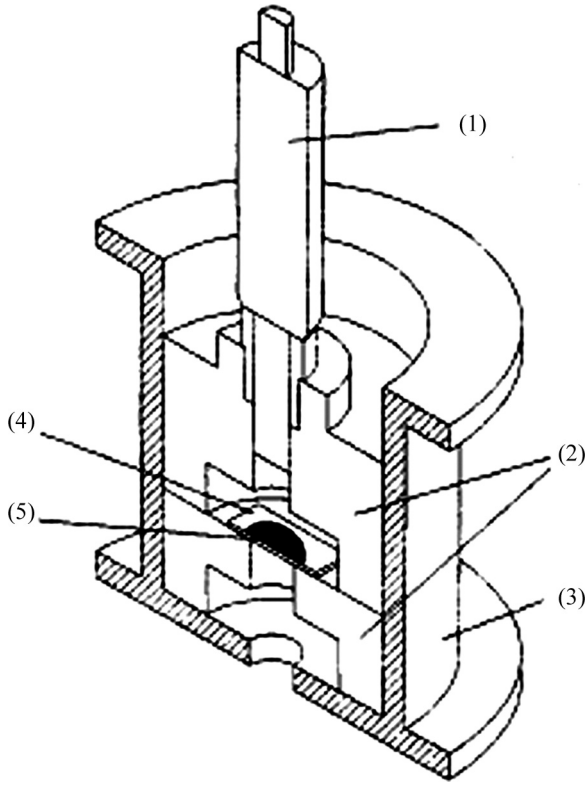

FIGURE 3 Schematic overview of the photopyroelectric measuring cell: (1) micrometer screw, (2) stainless steel positioners, (3) temperature controlled copper holder, (4) pyroelectrical transducer, (5) sample.

with f the modulation frequency, I_0 the laser light intensity, ρ_s, C_s and ρ_p, C_p respectively the density and heat capacity (per unit volume) of the sample, s, and the transducer, p. With this approximation, the phase of the pyroelectric signal is constant, and the amplitude is given by

$$|V(\omega)|_{norm} = H(\omega)\frac{\rho_p C_p L_p}{\rho_s C_s L_s + \rho_p C_p L_p} \tag{8}$$

with $H(\omega)$ an electrical transfer function.

A schematic overview of the setup as it was used for our experiments is shown in Figure 3. The measuring cell consists of two parts of stainless steel that can be fixed to each other. The pyroelectric

sensor on top of the lower part is placed so that the non illuminated parts are in good thermal contact with the cell. In the upper part, a micrometer screw is placed with its end parallel to the transducer. The temperature of the setup is controlled by a copper shield with a heating coil and a thermistor thermometer, close to the pyroelectric transducer. A second temperature controlled shield is put around the first one in order to shield temperature fluctuations in the laboratory. The setup can be operated from room temperature up to 100°C with a stability of 1 mK. By positioning the micrometer screw at different distances to the sample it is possible to arrive at absolute values of the specific heat capacity (per unit volume) [10]. In this study a large distance (effectively infinite) between the sample and the micrometer screw was kept constant. Therefore no absolute value of the specific heat capacity was obtained. The PPE AC calorimetric $c_p(T)$ data were rescaled with respect to those obtained by ASC.

3. EXPERIMENTAL RESULTS

3.1. The Nematic-Isotropic Phase Transition

The nematic-isotropic (N-I) phase transition is usually described by the Landau-de Gennes theory [12]. The free energy, $G(S,T)$, can be written as:

$$G = G_0 + \frac{1}{2}AS^2 + \frac{1}{3}BS^3 + \frac{1}{4}CS^4 + \cdots \tag{9}$$

with S, the nematic (macroscopic) order parameter, $A = a(T - T^*)$ and $a, T^*,\ B, C$ constants ($a, C > 0$ and T^* the lower temperature limit for the thermodynamic stability of the isotropic phase). The presence of the third order term in Eq. (9) implies the first order character of the N-I transition and a small value of B causes its weak character. Therefore the N-I phase transition is classified as a weakly first order one. Its latent heat in this mean-field model can be written as:

$$\Delta H_L = \frac{2aB^2T_{NI}}{9C^2}. \tag{10}$$

The nematic-isotropic phase transition in $\overline{10}O\bar{4}$ was investigated by means of ASC. The specific heat capacity near the N-I transition obtained from a heating run (10 mK/min) is shown in Figure 4. During this heating run the sample was stirred in order to optimize its homogeneity. The two-phase region is clearly visible and extends over approximately 240 mK. Figure 5 shows the enthalpy data as a function of temperature near the N-I transition, a linear background was

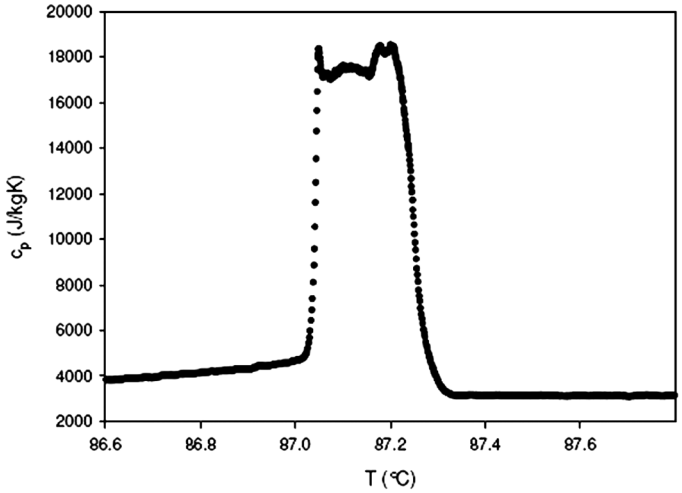

FIGURE 4 Specific heat capacity of $\overline{1}0\bar{4}$ near the N-I phase transition.

subtracted. From these enthalpy data, the latent heat of this weakly first order phase transition can be determined. It must be taken into account that the enthalpy increase in the two phase region consists of two parts: the latent heat, ΔH_L, and the heat needed to heat the

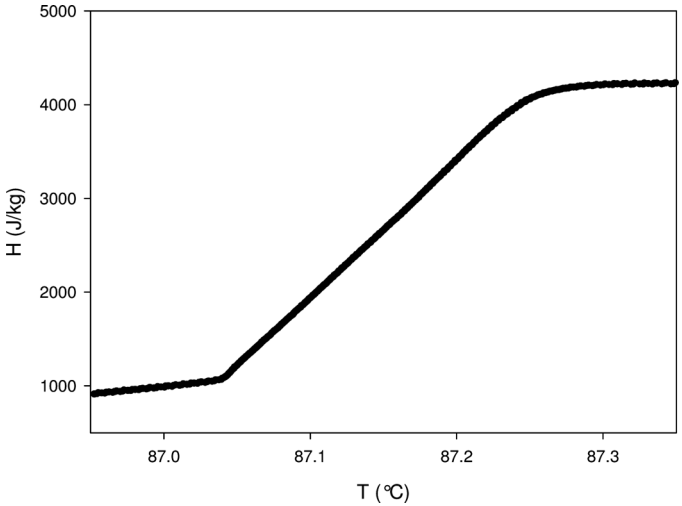

FIGURE 5 Enthalpy of $\overline{1}0\bar{4}$ near the N-I phase transition with a linear background subtracted.

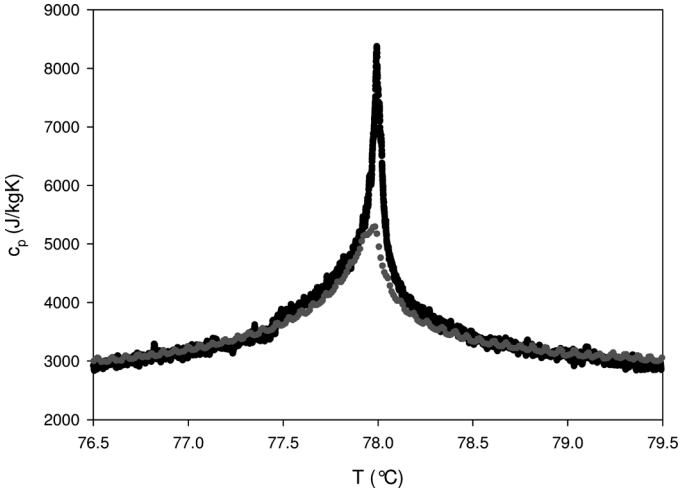

FIGURE 6 Comparison of the ASC (black) and PPE AC calorimetry (grey) specific heat capacity data as a function of temperature near the N-SmA phase transition temperature.

liquid crystal from the beginning to the end of the two phase region. The two phase region of this N-I transition is rather wide, so the latter contribution to the enthalpy increase is substantial, but it can be subtracted of by extrapolating the enthalpy curve into the two phase region. A latent heat of $\Delta H_L = 3.13 \pm 0.02\,\mathrm{J/g}$ was found.

3.2. The Nematic-Smectic A Phase Transition

The specific heat capacity data, $c_p(T)$, near the nematic-smectic A phase transition measured by means of the ASC technique are shown in Figure 6. A comparison between the ASC and PPE AC calorimetric results was also made in this figure. Since in this study no absolute values for $c_p(T)$ were obtained by means of PPE AC calorimetry, the latter $c_p(T)$ data were rescaled with respect to the $c_p(T)$ data obtained with ASC. The scanning rates for both runs were different: the ASC scan was made at a rate of 2 mK/min while the PPE AC calorimetric scan was made at a rate of 20 mK/min. Therefore the $c_p(T)$ peak obtained by means of PPE AC calorimetry is less sharp and smaller as the one obtained by ASC. Apart from this understandable difference there is good agreement between the $c_p(T)$ data for the two different measurement techniques.

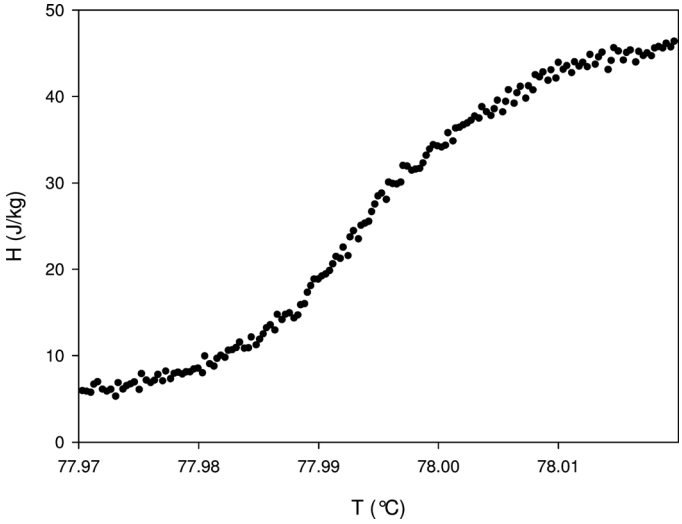

FIGURE 7 Enthalpy of $\overline{1}0O\bar{4}$ near the N-SmA phase transition with a linear background subtracted.

Figure 7 shows the enthalpy data near the N-SmA transition, a linear background was subtracted. After analyzing this figure an upper limit for the latent heat, ΔH_L of 3.10^{-3} J/g was found. Therefore this N-SmA phase transition may be classified as continuous one within our experimental resolution.

Generally, the effective specific heat critical exponent, α, is determined by fitting the power law which describes the specific heat capacity c_p:

$$c_p = A^{\pm}|\tau|^{-\alpha}(1 + D|\tau|^{0.5}) + B + E\tau, \tag{11}$$

with A^+, A^- the critical amplitudes respectively above and below the critical temperature T_c, $\tau = T - T_c/T_c$ the reduced temperature difference, D the amplitude of the first correction-to-scaling term, B a constant and $E\tau$ a linear background term. The problem with this fit expression is that all the different parameters are strongly correlated. A reduction of fit parameters therefore means better, more precise fit results.

In order to reduce the number of fit parameters a new quantity, C, is introduced:

$$C(T) = \frac{H(T) - H(T_c)}{T - T_c}. \tag{12}$$

C can be visualized as the slope of the chord connecting the point *(T, H)* with the critical point (T_c, H_c) on the *H(T)*-curve.

Integration of

$$c_p = A^{\pm}|\tau|^{-\alpha} + B, \tag{13}$$

the most simple form of the power law expression describing the specific heat capacity, with respect to the temperature T, gives an expression for *H(T)*. Substituting this in Eq. (12) gives:

$$C = \frac{A}{1-\alpha}|\tau|^{-\alpha} + B. \tag{14}$$

Since C and c_p have the same background term B, it is possible to eliminate the parameter B by subtracting c_p from C:

$$C - c_p = \frac{\alpha A}{1-\alpha}|\tau|^{-\alpha}. \tag{15}$$

Equation (15) makes it possible to determine the effective specific heat critical exponent, α, in a very simple way: the negative slope of $\log(C - c_p)$ versus $\log|\tau|$ plot gives α.

Although the application of this method looks very easy, care must be taken in the choice of the phase transition temperature T_c. The wrong choice of T_c can have drastic consequences on the course of

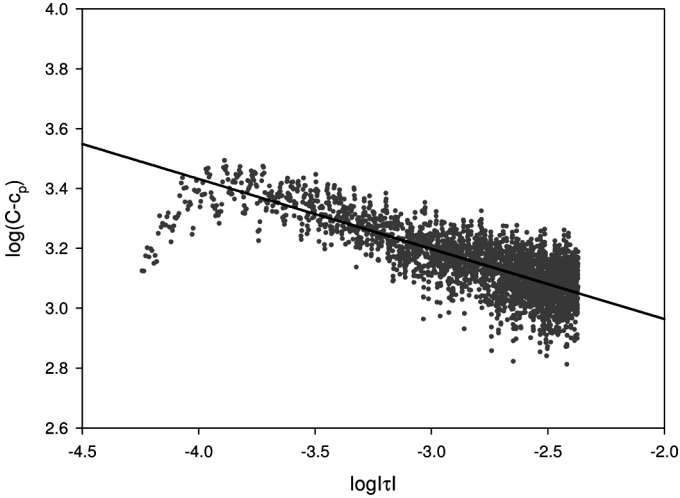

FIGURE 8 Plot of $\log(C - c_p)$ versus $\log|\tau|$ for $T > T_c$ (grey) and a linear fit (black) for the data in the range $-4 < \log|\tau| < -2.4$.

the *log-log* plots. For continuous phase transitions the correct phase transition temperature can be found by locating the inflection point in the *H(T)* data.

In Figure 8 the $\log(C - c_p)$ versus $\log|\tau|$ plot for the N-SmA phase transition in $\overline{1}0\bar{4}$ is given for the data above T_c together with a linear fit for the data in the range $-4 < \log|\tau| < -2.4$. The critical temperature, T_c, was found to be 77.990°C and the effective specific heat critical exponent was determined to be $\alpha = 0.23 \pm 0.01$, thus between the 3D XY and the tricritical value. Fitting of the data below T_c give consistent results. Efforts to include additional terms in Eq. 13 (correction terms) did not improve the quality of the fits.

4. CONCLUSIONS

In this article we investigated the liquid crystal $\overline{1}0\bar{4}$ with the emphasis on the nematic-to-smectic A and the nematic-to-isotropic phase transitions. The N-I phase transition was investigated by means of adiabatic scanning calorimetry (ASC), it could be classified as a weakly first order phase transition as predicted by the Landau-de Gennes theory [12] and the latent heat of this phase transition could be determined: $\Delta H_L = 3.13 \pm 0.02\,\mathrm{J/g}$.

ASC measurements on the N-SmA transition of $\overline{1}0\bar{4}$ showed that this was a continuous phase transition and the phase transition temperature, T_c, was found to be 77.990°C. The value of the effective specific heat capacity critical exponent was determined to be $\alpha = 0.23 \pm 0.01$, thus between the 3D XY and tricritical value. There was also good agreement between the ASC specific heat capacity results near the N-SmA transition and those obtained by means of a photopyroelectrical AC calorimetry technique also carried out in our laboratory.

REFERENCES

[1] Keller, E. N., Nachaliel, E., Davidov, D., & Böffel, C. (1986). *Phys. Rev. A*, *34*, 4363.
[2] Chan, T., Bahr, C., Heppke, G., & Garland, C. W. (1993). *Liq. Cryst.*, *13*, 667.
[3] Brauniger, T. & Fung, B. M. (1995). *J. Chem. Phys.*, *102*, 7714.
[4] Bahr, C. & Heppke, G. (1990). *Phys. Rev. Lett.*, *65*, 3297.
[5] Stanley, H. E. (1971). *Introduction to Phase Transitions and Critical Phenomena*, Oxford University Press: Oxford.
[6] Callen, H. B. (1985). *Thermodynamics and an Introduction to Thermostatistics*, Wiley: New York.
[7] Thoen, J. (1997). Thermal methods. In: *Physical properties of Liquid Crystals*, Demus, D., Goodby, J., Gray, G., Spiess, H. W., & Vill, V. (Eds.), Wiley-VCH: Weinheim, 208–232.

[8] Garland, C. W. (2001). Calorimetric studies. In: *Liquid Crystals: Experimental Studies of Physical Properties and Phase Transitions*, Kumar, S. (Ed.), Cambridge University Press: Cambridge, 240–294.
[9] Thoen, J., Bloemen, E., Marynissen, H., & Van Dael, W. (1982). In: *Proceedings of the Eighth Symposium on Thermophysical Properties, National Bureau of Standards, Maryland 1981*, Sengers, J. V. (Ed.), American Society of Mechanical Engineers: New York, 422–428.
[10] Caerels, J., Glorieux, C., & Thoen, J. (1998). *Rev. Sci. Instrum.*, *69*, 2452.
[11] Caerels, J., Glorieux, C., & Thoen, J. (2003). *Phys. Rev. E*, *65*, 031704.
[12] de Gennes, P. G. & Prost, J. (1993). *The Physics of Liquid Crystals.*, 2nd ed., Clarendon Press: Oxford.